

Featuring work on the plug-and-play production for safer antimicrobial activities from Prof. Jungho Hwang at School of Mechanical Engineering, Yonsei University, Seoul, Korea, Prof. Jong Oh Kim at College of Pharmacy, Yeungnam University, Gyeongsan, Korea, and Prof. Jeong Hoon Byeon at School of Mechanical Engineering, Yeungnam University, Gyeongsan, Korea.

Plug-and-play safe-by-design production of metal-doped tellurium nanoparticles with safer antimicrobial activities

The findings of this study offer a realizable on-demand system to produce safer antimicrobials using a plug-and-play device, and provide proof of concept for optimizations of material combinations and structures for a range of safe antimicrobial applications.

### As featured in:







See Jungho Hwang, Jong Oh Kim, Jeong Hoon Byeon *et al.*, *Environ. Sci.: Nano*, 2019, 6, 2074.

PAPER



Cite this: *Environ. Sci.: Nano*, 2019, 6, 2074

# Plug-and-play safe-by-design production of metal-doped tellurium nanoparticles with safer antimicrobial activities†

Dae Hoon Park, <sup>‡a</sup> Milan Gautam,<sup>‡b</sup> Sung Jae Park,<sup>a</sup> Jungho Hwang, <sup>\*a</sup> Chul Soon Yong,<sup>b</sup> Jong Oh Kim <sup>\*b</sup> and Jeong Hoon Byeon <sup>\*c</sup>

Safe-by-design principles, such as optimum balance of material function and safety, have received much recent attention. On-demand production is also receiving great interest in the realization of nanotechnologies that meet unpredictable demands of reconfiguration and modification to maximize the efficacy of materials processing. Antimicrobial nanomaterials are representative subjects of these approaches, because they require built-to-order configurations with safe-by-design principles for practical applications. However, few studies have achieved biosafety with original material function using economically feasible production platforms. In this regard, we developed a safe-by-design plug-and-play approach for continuous gas flow production of silver (or copper)-doped tellurium (Ag- or Cu-Te) nanoparticles with safer antimicrobial activity. Using this approach, we achieved precise modulation of dopant contents (5–8% atomic Ag and Cu) in nanoparticles without using batch hydrothermal chemistry. We also suggest the use of ratios between biocompatibility and antimicrobial activity as safety indices (SIs) for evaluations of nanoparticle applications. Approximately 6% atomic Ag in Ag–Te particles exhibited an optimal SI and significantly reduced the minimum inhibitory concentration of individual Te nanoparticles.

Received 1st April 2019,  
Accepted 16th May 2019

DOI: 10.1039/c9en00372j

rsc.li/es-nano

## Environmental significance

Recently, functional nanoscale compounds have been scrutinized to avoid fatal toxicities during their use as antimicrobial agents. However, metal nanoparticles and ionic nanocomplexes have been widely used to dissolve metallic ions in biologically contaminated sites and to prevent harmful impacts on humans and the environment. To achieve a trade-off of antimicrobial materials, safe-by-design approaches have been considered, and polymer coatings have been primarily employed to improve the safety of antimicrobial agents. However, instability and hydrolysis and weak bonds between metals and polymers warrant the development of alternative designs for the fabrication of more stable compounds with antimicrobial activity and biological safety. Thus, we developed a plug-and-play technique to produce safer antimicrobial nanoparticles without significant toxicity or process complexity, and with ratios of biocompatibility and antimicrobial activity (safety index, SI) that allow a realizable platform for the optimal use of antimicrobials. Specifically, we constructed a 4-rod spark ablation system comprising three silver (or copper) anodes with a tellurium cathode to produce silver- or copper-doped tellurium nanoparticles using a compact, controllable, and reconfigurable process. Due to the doping effect, minimal inhibitory concentrations of base tellurium and cytotoxicities of individual silver or copper were dramatically reduced, as indicated by the significantly increased SI.

## Introduction

Antimicrobial compounds have been used in numerous hygiene and healthcare applications, including consumer products that prevent biohazards, such as infections with patho-

genic bacteria. Currently, more than 70% of bacterial infections are resistant to conventionally used antibiotics, such as tetracycline and ampicillin,<sup>1,2</sup> and alternative highly active antibacterial agents are urgently needed. Metallic nanoparticles and nanocomposites have potential as antimicrobial agents, particularly because the dissolution of metal particles and release of metal ions enhance the antimicrobial efficacies, even in multiresistant bacteria.<sup>3–8</sup> Among metal nanoparticles, silver (Ag) and copper (Cu) nanoparticles are the best characterized antimicrobial agents, and are widely used in cosmetics, sprays, textiles, deodorants, and medicines for the prevention of infection. Antimicrobial activities of Ag and Cu particles against Gram-positive and -negative bacterial strains are associated with the dissolution of ions

<sup>a</sup> School of Mechanical Engineering, Yonsei University, Seoul 03722, Republic of Korea. E-mail: hwangjh@yonsei.ac.kr

<sup>b</sup> College of Pharmacy, Yeungnam University, Gyeongsan 38541, Republic of Korea. E-mail: jongohkim@yu.ac.kr

<sup>c</sup> School of Mechanical Engineering, Yeungnam University, Gyeongsan 38541, Republic of Korea. E-mail: postjb@yu.ac.kr

† Electronic supplementary information (ESI) available. See DOI: 10.1039/c9en00372j

‡ These authors contributed equally to this work.



that facilitate electrostatic interactions with negatively charged bacterial membranes, and induce injury by damaging proteins and membranes, thus inducing oxidative stress.<sup>9,10</sup>

Significant toxic side effects of Ag and Cu nanoparticles have been considered for humans and the environment, and have been associated with cell uptake and entry into lysosomes,<sup>11,12</sup> and subsequent production of reactive oxygen species (ROS) that damage DNA.<sup>13,14</sup> These observations have complicated the selection of antimicrobials, and have prioritized the balance of antimicrobial function and bio-environmental safety.<sup>15</sup> Moreover, health and environmental hazards of materials processes need to be resolved,<sup>16</sup> warranting safe-by-design approaches that favor the trade-off between materials functions and toxicities.<sup>17</sup> Safe-by-design nanoparticles are conventionally produced using surface coatings with polymeric compounds, such as polyethylene glycols and chitosan chelates. However, hydrolysis and intrinsic toxicities of these agents have limited their safety and practicality.<sup>18</sup> In more recent studies, surface modifications have been investigated to reduce nanoparticle toxicity without significant loss of function<sup>19–21</sup> and these have resulted in inert surfaces that can be placed in direct contact with biological systems.<sup>22,23</sup> In particular, the effects of metal doping of base materials on the dissolution kinetics of metallic nanoparticles have been exploited to reduce toxic effects of nanoparticles,<sup>24–28</sup> although few studies have specifically validated the desired functions and biotoxicities of metallic nanoparticles. Hence, practical applications of safe-by-design approaches are currently limited to basic studies of dopants, Fe, Al, Ti, and S, and developments of these technologies are urgently needed.

In this study, we addressed two major issues of the safe-by-design approach, and developed a plug-and-play nanoparticle production system that can be used to adjust compositions and safety indices (SIs). Specifically, Ag or Cu-doped tellurium (Te; Ag–Te or Cu–Te) nanoparticles with different Ag

or Cu atomic contents were prepared using a 4-rod spark ablation device that can be used for continuous production. Te was used as the base component of the present nanoparticles, because antimicrobial activities of relatively non-toxic  $\text{TeO}_3^{2-}$  ions have been shown against Gram-negative bacteria, such as *Escherichia coli* (*E. coli*), *Pseudomonas aeruginosa*, *Salmonella typhi*, and *Klebsiella pneumonia*,<sup>29–32</sup> although the effects of  $\text{TeO}_3^{2-}$  ions on Gram-positive bacteria and biocompatibilities with mammalian cells remain unclear. Unlike previous safe-by-design nanoparticles, we maximized antimicrobial activity without increasing toxicity by regulating atomic contents of Ag (or Cu) from 5% to 8% referring to previous reports,<sup>25–28</sup> and identified process conditions that optimize the balance of antimicrobial activity with toxicity. The present spark ablation device comprises three Ag (or Cu) anodes and a Te cathode in a compact chamber of 8 cm<sup>3</sup> containing pure nitrogen. Electrodes were connected to an alternating current (AC) power supply (voltage and frequency adjustable), and bipolar charged Ag (or Cu) and Te vapors from AC electric fields were rapidly co-condensed *via* electrostatic attractions under conditions of a nitrogen gas flow and a high temperature gradient, leading to direct insertion of Ag (or Cu) vapors into molten Te to form Ag–Te or Cu–Te nanoparticles (Fig. 1, refer to the ESI† for the experimental details). This plug-and-play route allows production of nanoparticles with precisely controlled Ag or Cu contents without the use of hydrothermal chemistries and post-treatments. The resulting nanoparticles were collected electrostatically and dispersed in buffered saline, and were then employed without further purification in assays of antimicrobial activity against *E. coli* (Gram negative) and *Staphylococcus epidermidis* (*S. epidermidis*; Gram positive) strains and biocompatibility in human dermal fibroblasts (HDFs; Fig. S1, ESI†). Estimated ratios between biocompatibilities and antimicrobial activities were used to determine the SI and identify safe-by-design parameters that allow safer use of antimicrobials.



**Fig. 1** Schematic of spark ablation to form Ag or Cu-doped Te nanoparticles from three Ag or Cu anodes (green) and a Te cathode (red) inside a chamber under a nitrogen gas flow and an AC electric field; high temperature spark channels induced evaporation of electrode metals, and the resulting vapors with bipolar charges were then co-condensed over the temperature gradient caused by the gas flow, resulting in the direct insertion of Ag or Cu into Te. Precise adjustments of Ag or Cu contents in the produced particles were achieved by varying the number of operating anodes (1–3), and by exploiting differences in thermophysical properties, such as heat of vaporization between Te and Ag and Cu.

## Results and discussion

Size distributions of particles were measured using a scanning mobility particle sizer (SMPS; 3936, TSI, USA) by direct sampling of the particle-laden flow. Fig. S2a–c (ESI†) show the distributions of Ag–Te and Cu–Te particles and individual Te particles. The geometric mean diameters (GMDs) of the particles were less than 200 nm, and the geometric standard deviations and total number concentrations were 1.59–1.65 and  $1.5 \times 10^7$ – $2.1 \times 10^7$  particles per  $\text{cm}^3$ , respectively. Compared with Te alone, Ag- and Cu-doped configurations did not significantly alter the unimodal distribution of Te alone, and similarities in size distributions between individual Te and Ag- or Cu-doped particles represent Te dominant configurations, reflecting the properties of spark ablation. These ablation conditions were designed to induce imbalances of Te and Ag or Cu contents to reduce toxicity by moderating the contents of Ag or Cu, which are more toxic than Te. These controls were achieved by exploiting differences in heats of vaporization between Te ( $52.55 \text{ kJ mol}^{-1}$ ), Ag ( $250.58 \text{ kJ mol}^{-1}$ ), and Cu ( $300.30 \text{ kJ mol}^{-1}$ ). Size distributions did not differ significantly between nanoparticles that were produced with 1 to 3 Ag or Cu anodes, suggesting complete insertion of Ag or Cu into base Te due to the coincidence of + and – charges and electrostatic attractions between vapors during the process. Size distributions were also determined in phosphate buffered saline (PBS) using dynamic light scattering (DLS, Nano ZS, Malvern Instruments, UK) analyses (Fig. S2d, ESI†). Although size distributions varied more with higher particle concentrations after 30 min collection in 2 mL of PBS than in SMPS measurements, size ranges of Ag–Te (or Cu–Te) particles did not differ significantly with those of Te, even in the absence of stabilizing agents, indicating that Te remained the dominant constituent. To confirm the dominance of Te, scanning electron microscopy-energy dispersive

X-ray (SEM-EDX; S-4800, Hitachi, Japan) mapping microanalyses were performed to measure the atomic Ag and Cu contents in particles (Fig. S3, ESI†). In these analyses of Ag and Cu distributions in Ag–Te and Cu–Te particles, Ag and Cu were present at 5.4% and 6.1%, 6.8% and 6.9%, and 8.0% and 7.7% of Te contents following the use of 1, 2, and 3 operating Ag or Cu anodes, respectively.

Morphologies and microstructures of Ag–Te and Cu–Te particles were compared with those of Te, Ag, and Cu particles using transmission electron microscopy (TEM; Tecnai G<sup>2</sup> F20 S-TWIN, FEI, USA). As shown in Fig. 2, spark ablation processes produced primary spherical Te, Ag, and Cu conglomerates, although differences in particle sizes (Te,  $24 \pm 6.6 \text{ nm}$ ; Ag,  $4.4 \pm 1.3 \text{ nm}$ ; Cu,  $4.2 \pm 0.9 \text{ nm}$ ) reflected differing degrees of metal vaporization and condensation. The high-magnification TEM images of Te showed a  $d$ -spacing of 0.590 nm, indicating the formation of (001) hexagonal Te planes,<sup>33,34</sup> and confirming that spark ablation produces crystalline Te particles. Characteristically, the  $d$ -spacing values of Ag and Cu particles were 0.234 and 0.213 nm, respectively, suggesting the formation of Miller (111) planes from face-centered cubic Ag and Cu. However, Ag- and Cu-doping in the presence of 2 Ag or Cu anodes led to the formation of another type of conglomerate, which was distinguishable from that produced in the presence of 1 or 3 anodes. Specifically, microstructures of Ag–Te and Cu–Te particles comprised (001) hexagonal Te planes with  $d$ -spacings of 0.374 and 0.367 nm, respectively. These results corresponded to (110)-directed monoclinic Ag<sub>2</sub>Te (ref. 34 and 35) and (002)-directed hexagonal Cu<sub>2</sub>Te phases,<sup>36,37</sup> respectively, suggesting that co-condensation of Ag (or Cu) and Te atoms induces strong incorporation of Ag and Cu ions into Te and the formation of partial alloys with dendritic structures. As shown in Fig. S4a,† the dendritic nature was also observed for other Ag–Te and Cu–Te particles with different Ag (5.4% and 8.0% of Ag) and

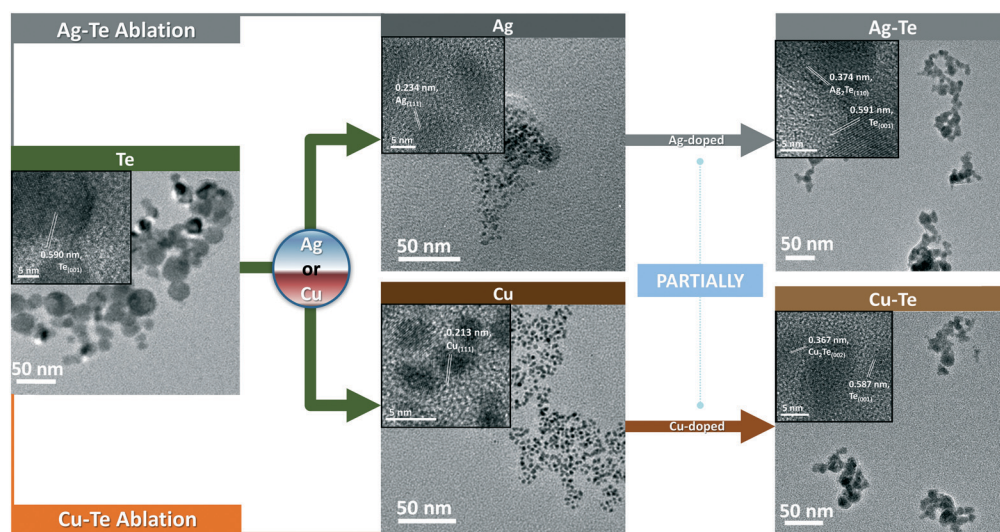


Fig. 2 High- and low-magnification TEM images of Ag–Te, Cu–Te, Te, Ag, and Cu particles; particles from spark ablation were directly deposited on a carbon-coated copper grid. Images of Ag–Te and Cu–Te are from operations with the two Ag or Cu electrodes, because no distinguishable morphological differences were identified between Ag–Te and Cu–Te spark configurations.

Cu (6.1% and 7.7% of Cu) contents. Hence, partial doping affected the Te crystal growth during the present process and led to different sizes ( $14 \pm 4.3$  nm for Ag-Te and  $12 \pm 3.5$  nm for Cu-Te in TEM observation) and shapes of conglomerates compared with Te alone, suggesting that spark ablation can be used to precisely produce partially doped metallic nanoparticles in a plug-and-play manner. The morphological changes from the conglomeration based on the partial doping of Ag or Cu may also affect the slight size increases in SMPS and DLS analyses (Fig. S2†) because the doping induces different crystal growth from the Te alone configuration that causes the formation of dendritic structures for Ag-Te and Cu-Te configurations. Thus, the size increases by increasing the atomic Ag or Cu content (*i.e.*, inducing greater frequencies of doping) may be due to the formation of larger dendritic structures. Fortunately, this structure might be suitable for demonstrating strong antimicrobial activities because the membrane damage of bacterial cells could be promoted by dendritic particles.<sup>38,39</sup> The valence states of Ag-Te and Cu-Te particles with doublet shifts in the Te3d, Cu2p, and Ag3d core spectra were consistent with partial formation of Ag<sub>2</sub>Te and Cu<sub>2</sub>Te when compared with the doublets of Te and standard Ag and Cu particles (Fig. S4b, ESI†), supporting further the partial formation of Ag<sub>2</sub>Te or Cu<sub>2</sub>Te on base Te particles during co-condensation (observed in Fig. 2). In addition, analyses of X-ray photoelectron spectroscopy (XPS; Axis-HIS, Kratos Analytical, Japan) peaks showed Ag and Cu contents of 5.3% and 5.9%, 6.5% and 6.6%, and 8.0% and 7.8% in particles produced with 1, 2, and 3 operating Ag or Cu anodes, respectively. These data further indicate that precise modulation of spark ablation can be used to achieve a desired range (5–8%) of atomic Ag and Cu contents. Moreover, in the comparisons of UV-vis spectrophotometric (T60, PG Instruments, UK) properties of Ag-Te and Cu-Te particles (Fig. S4c, ESI†), Ag and Cu-doped configurations did not exhibit Te-characteristic absorption at 350 nm, further indicating crystalline transformations of Te. Moreover, Ag-Te and Cu-Te particles did not absorb visible light (390–700 nm) significantly, indicating that the produced particles may also be suitable for transparent antimicrobial coatings.<sup>38</sup> In analyses of zeta potentials in PBS at pH 7.4 and acetate buffered saline at 5.5 (Fig. S4c, ESI†), dispersion images of Ag-Te, Cu-Te, and Te particles showed no significant changes in zeta potentials or dispersion colors following partial doping with Ag and Cu.

In further experiments, antibacterial activities of Ag-Te and Cu-Te particles were evaluated and compared with those of individual Te, Ag, and Cu particles in *E. coli* and *S. epidermidis*. As shown in Fig. 3a, Ag and Cu particles exhibited >99.9% antimicrobial efficiency against both bacterial strains, whereas Te had >80% activity against *E. coli* and was inactive against *S. epidermidis*, suggesting that Te particles lack efficacy against Gram-positive bacteria and Ag or Cu dramatically enhances the activity against *S. epidermidis*. To quantitatively assess antibacterial activities, we calculated the minimal inhibitory concentrations (MICs) of the particles

(Fig. 3b). In all cases, MICs were higher in *S. epidermidis* than in *E. coli*, likely reflecting the greater resistance of thicker and more complex peptidoglycan layers.<sup>31,40,41</sup> Correspondingly, the MIC of Te particles was about  $8000 \mu\text{g mL}^{-1}$  against *S. epidermidis* and those of Ag and Cu particles were 62.50 and  $125.00 \mu\text{g mL}^{-1}$ , respectively, as confirmed by confocal laser scanning microscopy (CLSM; LSM 880, Carl Zeiss, Germany; insets of Fig. 3b) analyses at a concentration of  $30 \mu\text{g mL}^{-1}$  (the effective concentration to inhibit the growth of both *E. coli* and *S. epidermidis*). These MICs show that Ag and Cu doping dramatically improves the antibacterial activity of Te nanoparticles, even *S. epidermidis*. Furthermore, Ag-Te and Cu-Te particles had lower MICs against *E. coli* than Ag and Cu particles, indicating that doping with Ag or Cu can significantly enhance the antimicrobial activity of Te following the release of Ag<sup>+</sup> or Cu<sup>2+</sup> with TeO<sub>3</sub><sup>2-</sup> that synergistically impairs membrane functions.<sup>31,42</sup> In addition, adjustments of atomic Ag and Cu contents between 5% and 8% in Ag and Cu-doped particles may maximize the activity of Te by preventing aggregation of Ag or Cu.<sup>43</sup> This tendency was further confirmed by the disc diffusion method at an areal density of  $30 \mu\text{g cm}^{-2}$  (Fig. S5†), which exhibits the inhibition zone width (IZW) of bacterial growth on a plate medium. Both Ag-Te- and Cu-Te-deposited disc specimens clearly showed greater activities for inhibiting bacterial growth than individual Ag, Cu, and Te particles. To confirm these enhancements in the antimicrobial activities of Ag-Te and Cu-Te particles, differences in the cell morphology between untreated and Ag-Te- and Cu-Te-treated *E. coli* and *S. epidermidis* were analyzed using low- and high-magnification SEM (JSM-7800F, JEOL, Japan) (Fig. 4a and b). These analyses showed distortion of smooth ellipsoidal and spherical morphologies after particle treatments, likely reflecting impaired membrane functions. The high-magnification SEM images also showed the presence of Ag-Te and Cu-Te particles around bacterial cells, suggesting that close contact of cells and particles induces irreversible cell damage and leads to cell death. The corresponding CLSM images of the particle-treated bacteria (lower panels of Fig. 4a and b) exhibited no green fluorescence of viable cells.

To assess the toxicities of Ag-Te and Cu-Te particles, HDF cell viability was estimated using 3-(4,5-dimethylthiazol-2-yl)-2,5-diphenyltetrazolium bromide (MTT) assays after 24- and 48 h treatments with particles at  $5\text{--}200 \mu\text{g mL}^{-1}$  (Fig. 5). Ag and Cu particles were toxic to HDF cells, with cell viabilities of 70.3% and 47.3%, respectively at 48 h, likely reflecting the production of free radicals and ROS.<sup>44</sup> In contrast, Ag-Te particles exhibited negligible toxicities at both time points, and were comparable to Te particles in these assays, suggesting sustained or controlled release of Ag ions from Ag<sub>2</sub>Te.<sup>45</sup> However, Cu-Te particles were more toxic than Ag particles, potentially due to the deleterious effects of Cu-mediated ROS generation.<sup>46</sup> Accordingly, the Cu-Te toxicity increased with Cu contents (Fig. S5, ESI†). Thus, to assess oxidative stress due to particle treatments, we performed assays using the ROS sensitive dye dichlorodihydrofluorescein diacetate



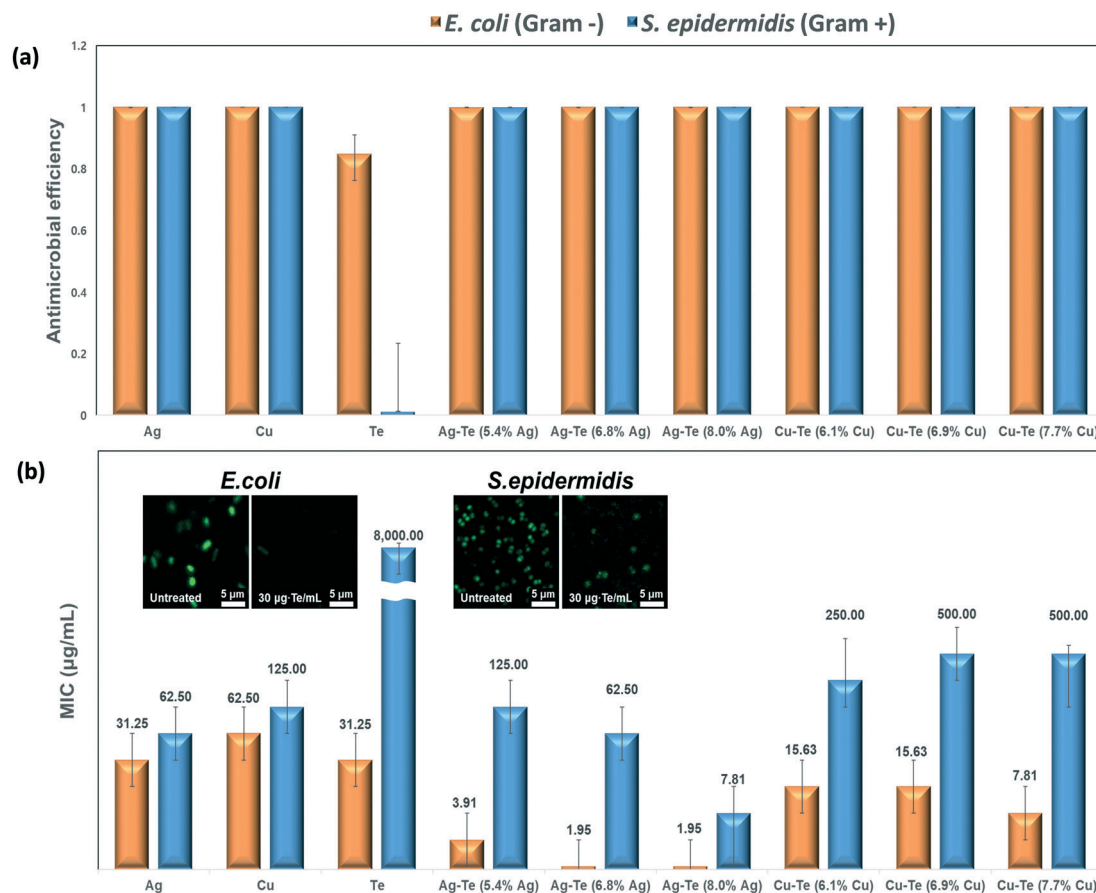


Fig. 3 Antimicrobial activities of Ag–Te, Cu–Te, Te, Ag, and Cu particles; upper and lower panels show the (a) antimicrobial efficiency and (b) MIC of particles against *E. coli* (Gram-negative) and *S. epidermidis* (Gram-positive). Insets of (b) show the CLSM images of viable (green fluorescence) *E. coli* and *S. epidermidis* strains with and without Te treatments ( $30 \mu\text{g mL}^{-1}$ ).

(DCFH-DA; Fig. 6), which detects intracellular ROS. In these experiments, 24 h treatments with Cu–Te particles led to higher ROS production than treatments with Ag–Te particles at  $50 \mu\text{g mL}^{-1}$ , which might be due to higher activities of released Cu ions from Cu–Te particles for the reduction of en-

zymatic activity.<sup>42</sup> Whereas low ROS levels reportedly activate cellular defense mechanisms, high levels promote oxidative stress and can damage lipids, proteins, and DNA irreversibly.<sup>47</sup> Thus, the present determinations of ROS and cell viability suggest that the latter conditions prevail in the

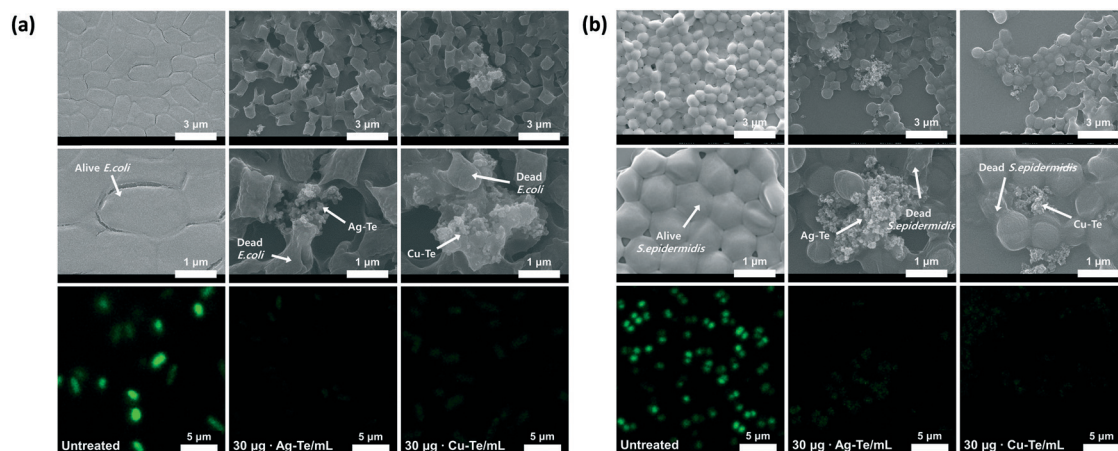


Fig. 4 Comparisons of bacterial morphologies from high- and low-magnification SEM images (upper) and CLSM evaluations of cell viability (lower) between the absence (left) and the presence of Ag–Te (middle) or Cu–Te (right) particles at  $30 \mu\text{g mL}^{-1}$ ; data are presented from *E. coli* (a, Gram-negative) and *S. epidermidis* (b, Gram-positive) strains with particles that were produced using 2 Ag or Cu anodes.

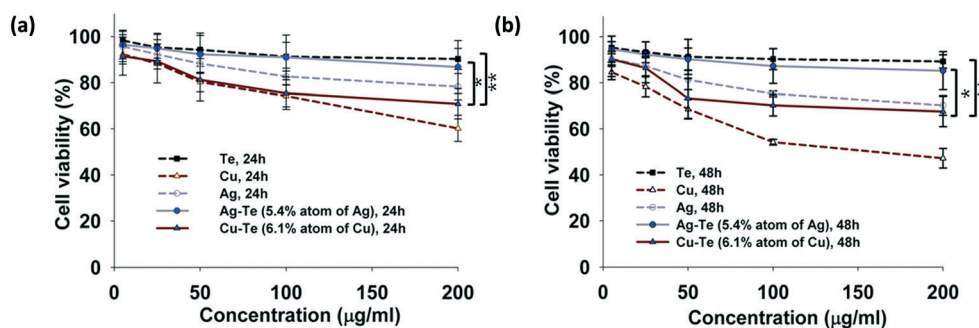


Fig. 5 Cytotoxicities of Ag-Te, Cu-Te, Te, Ag, and Cu particles produced using 2 Ag or Cu anodes after (a) 24 h and (b) 48 h incubation with HDF cells at particle concentrations of 5–200  $\mu\text{g mL}^{-1}$ ; \* $p < 0.05$ , \*\* $p < 0.01$ .

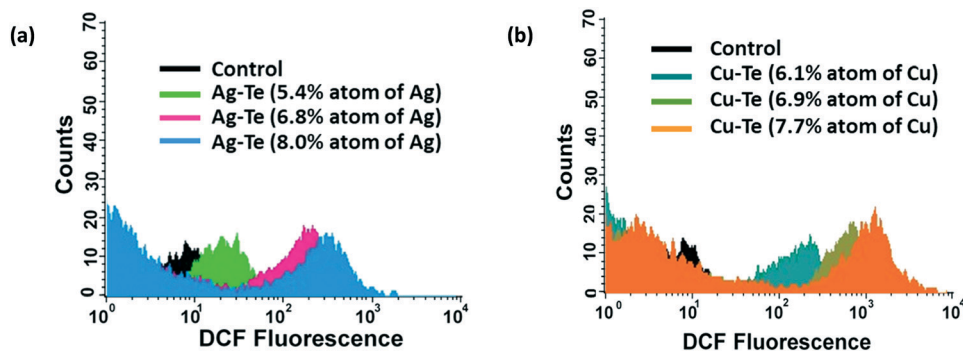


Fig. 6 ROS generation in HDF after 24 h treatments with (a) Ag-Te particles that were produced using 1, 2, and 3 Ag anodes and (b) Cu-Te particles that were produced using 1, 2, and 3 Cu anodes at 50  $\mu\text{g mL}^{-1}$ .

presence of Cu-Te particles. In agreement, hemolysis assays of defibrinated blood after 30 min treatments with particles (Fig. 7) showed significantly greater hemolysis in the presence of Cu-Te particles than that of Ag-Te particles ( $p < 0.001$ ), 76% hemolysis at 50  $\mu\text{g mL}^{-1}$ . Ag-Te particles caused less than 9% hemolysis at the same concentration, indicating potential as safe agents for antimicrobial applications. Moreover, these toxicity assays show that 6% atomic Ag in Te particles provides safe antimicrobial activity, with biocompatibility at all MICs for both bacteria.

To validate Ag-Te and Cu-Te particles, corresponding SIs were estimated using the following formula:

$$\text{SI} = \frac{\text{PC}_{90}}{\text{MIC}} \quad (1)$$

where  $\text{PC}_{90}$  is the particle concentration ( $\mu\text{g mL}^{-1}$ ) at >90% cell viability in MTT assays. The >90% cell viability in the equation is selected because >80% cell viability of nano-materials is generally workable for further biomedical investigation.<sup>48</sup> Estimated SIs were then plotted against number of operating anodes (Ag or Cu), and  $x$  (MIC)– $y$  ( $\text{PC}_{90}$ ) plots were generated to show the concentration ranges of safe-by-design antimicrobials against *E. coli* and *S. epidermidis* (Fig. 8). The data in the upper panels indicate that the higher SIs adhere to safe-by-design principles, whereas the lower SIs in the right-upper quadrant offer greater safety in antimicrobial ap-

plications. These plots indicate that approximately 6% atomic Ag provides an appropriate platform for identification of optimal antimicrobials for safe and practical use. In addition, the

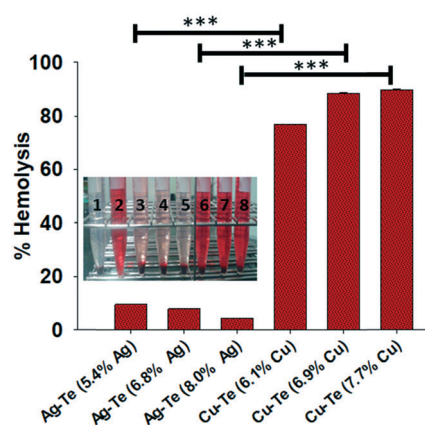


Fig. 7 Percentage hemolysis in RBCs after 30 min treatments with 50  $\mu\text{g mL}^{-1}$  Ag-Te and Cu-Te particles at 37 °C; the inset digital image shows hemoglobin in RBC supernatants after treatments with particles. Absorbance values were determined at 540 nm using a UV-spectrophotometer; \*\*\* $p < 0.001$ . Sample numbers 1–8 in the inset represent the negative control, the positive control, Ag-Te with 5.4% atomic Ag produced using 1 Ag anode, Ag-Te with 6.8% atomic Ag produced using 2 Ag anodes, Ag-Te with 8.0% atomic Ag produced using 3 Ag anodes, Cu-Te with 6.1% atomic Cu produced using 1 Cu anode, Cu-Te with 6.9% atomic Cu produced using 2 Cu anodes, and Cu-Te with 7.7% atomic Cu produced using 3 Cu anodes, respectively.

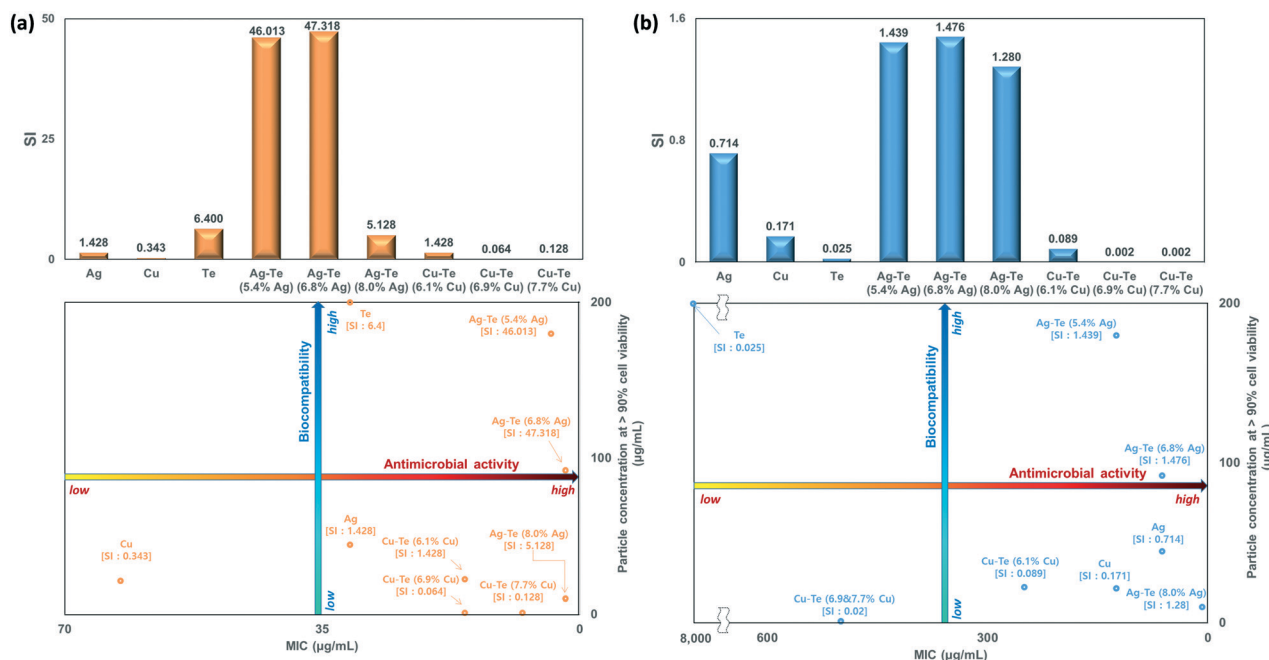


Fig. 8 SI values (upper) and ranges (lower) from estimations of antimicrobial activity (MIC) and biocompatibility (PC<sub>90</sub>) of Ag-Te and Cu-Te particles, and individual Te, Ag, and Cu particles. All experiments were performed using *E. coli* (a, Gram-negative) and *S. epidermidis* (b, Gram-positive) strains.

proposed heterogeneous spark ablation system provided greater production rates (0.158 g h<sup>-1</sup> for Ag-Te and 0.155 g h<sup>-1</sup> for Cu-Te) than those from individual Ag and Cu particles (0.001–0.1 g h<sup>-1</sup>) from homogenous spark ablations under the same specific energy consumption.<sup>49</sup> Finally, the present multi-electrode spark ablation method comprises a compact reconfigurable system that offers precise controls over elemental compositions of metallic antimicrobials.

## Conclusions

A plug-and-play safe-by-design approach was developed for continuous flow production of Ag and Cu-doped Te nanoparticles, and the resulting particles were assessed in terms of SIs to identify parameters of antimicrobial safety. The spark ablation device was designed with three Ag or Cu anodes and a Te cathode inside a compact chamber, and a pure nitrogen gas flow was passed through the chamber to carry the resulting particles. Atomic Ag and Cu contents in particles were precisely controlled between 5% and 8% by varying the number of operating anodes (1–3) connected to the high frequency AC power supply. Relatively small Ag or Cu contents induced the partial formation of Ag<sub>2</sub>Te or Cu<sub>2</sub>Te on base Te particles during co-condensation of bipolar charged Ag or Cu and Te vapors. The SIs from antimicrobial and toxicity assays were further estimated for the different Ag or Cu contents. These analyses indicated that 6% atomic Ag in particles is associated with an optimal SI and decreased MIC of Te, and no significant ROS production or hemotoxicity was observed. These findings indicate the feasibility of plug-and-

play continuous flow production with adjustable metal doping for the production of safe-by-design antimicrobials, offering a compact, reconfigurable, and digitizable platform for on-demand antimicrobials and a methodological concept for ensuring the safety of newly developed materials for practical applications.

## Methods

### Production of Ag (or Cu)-doped Te (Ag-Te or Cu-Te) nanoparticles

The spark ablation device comprised three Ag (AG-402561, Nilaco, Japan) or Cu (CU-112564, Nilaco, Japan) anodes of 3 mm in diameter and a Te (TE-E-035M-R, American Elements, USA) cathode of 6 mm in diameter. The electrodes were installed inside a chamber (8 cm<sup>3</sup>) and were connected to an AC high voltage-frequency power supply (2 kV, 2.5 kHz), as shown in Fig. S1.† The gap distance between Te and Ag (or Cu) electrodes was maintained at 1 mm inside the chamber, and the spark channel was formed between the electrodes under room temperature nitrogen (99.9999% purity) with a gas flow of 1.57 L min<sup>-1</sup>. The high temperature of the spark channel induced partial evaporation of electrodes, and Te and Ag or Cu vapors were subsequently co-condensed into solid Ag-Te or Cu-Te nanoparticles over the temperature gradient. The Ag or Cu contents in the produced particles were modulated by varying the number of operating Ag or Cu electrodes between 1 and 3, leading to atomic Ag or Cu percentages of precisely 5% to 8%. This range was sufficient to retain appropriate SI values from antimicrobial and cytotoxic assessments. To directly collect Ag-Te or Cu-Te particles, a



pin-to-ring type corona charger (+1.6 kV cm<sup>-1</sup>) was installed at the downstream of the ablation device and was used to induce + field charging of particles. Charged particles were then collected as powders on a polished stainless steel rod with a negative electric field of -0.8 kV cm<sup>-1</sup>. The particle collection rod was then inserted into a vial containing buffered saline, and the vial was then immersed in an ultrasonic bath for 10 min to suspend the particles in saline.

### Characterization

Size distributions of Ag-Te, Cu-Te, and Te particles in gaseous and aqueous states were measured using SMPS (3936, TSI, USA) and DLS (Nano-ZS, Malvern Instruments, UK) systems, respectively. SMPS measurements were performed by direct sampling of the particle-laden gas (0.3 L min<sup>-1</sup>) downstream of the ablation device. DLS assessments were conducted with particles suspended in buffered saline after 30 min particle collection on the sampling rod. To analyze the morphologies and microstructures of particles, a carbon-coated copper grid (Tedpella, USA) was placed on the holder of a grid sampler (Ineris, France), and the particle-laden flow was directly injected into the sampler to directly deposit the particles on the grid surface. The grid was then transferred to a holder for TEM analyses (Tecnai G<sup>2</sup> F20 S-TWIN, FEI, USA). The particle collection grid was also placed on a holder for SEM-EDX (S-4800, Hitachi, Japan) mapping analyses, and particle morphologies and elemental compositions were observed. The surface structures of Ag-Te and Cu-Te were assessed using XPS (Axis-HIS, Kratos Analytical, Japan), and the results were compared with those from pure Te, Ag, and Cu particles. Light absorption spectra of Ag-Te or Cu-Te particles in buffered saline were determined using a UV-vis spectrophotometer over the wavelength range of 300–1200 nm (T60, PG Instruments, UK).

### Bioassay

To exclude the surfactant influence for bioassays, the prepared Ag-Te and Cu-Te powders were directly dispersed in aqueous media just before the assays to avoid their coagulation and subsequent sedimentation. The antibacterial activities of the present particles against *E. coli* (ATCC-11775) and *S. epidermidis* (ATCC-14990) were evaluated using the colony counting method. Briefly, bacterial cultures were diluted to 10<sup>5</sup> CFU mL<sup>-1</sup> by measuring the optical densities at 620 nm using a UV-vis spectrophotometer. Subsequently, 100 µL aliquots of particle suspension were added to 2 mL bacterial solutions and were placed in a shaking incubator at 37 °C for 24 h. The incubated solutions were then diluted with deionized water to render appropriate concentrations for colony counting. Solutions were then spread on agar plates and were successively cultured at 37 °C for 24 h. The antimicrobial efficiency of particles was estimated using the following equation:

$$\eta_{\text{antimicrobial}} = 1 - \frac{\text{CFU}_{\text{treated}}}{\text{CFU}_{\text{untreated}}} \quad (2)$$

where CFU<sub>treated</sub> and CFU<sub>untreated</sub> are the resulting CFUs from treated and untreated configurations, respectively. To confirm the antimicrobial activities, bacteria (10<sup>5</sup> CFU mL<sup>-1</sup>) were incubated with a tryptic soy broth (TSB) medium containing particles at 30 µg mL<sup>-1</sup> for 1 h at 37 °C. Treated bacteria were then washed and resuspended in deionized water, and 5 µL drops were fixed onto silicon wafers (Tedpella, USA). The samples were then dried in ambient air and were placed on a holder for SEM (JSM-7800F, JEOL, Japan) analyses after thin platinum coating. Particle (30 µg mL<sup>-1</sup>)-treated bacteria were also incubated under gentle rotation at 37 °C for 1 h and were stained using LIVE/DEAD BacLight bacterial viability kits (L7012, Invitrogen, USA). Viable bacteria were indicated by green fluorescence and were visualized using CLSM (LSM 880, Carl Zeiss, Germany) to confirm the antimicrobial activities of particles. The MICs of the particles against bacteria were determined using the broth microdilution method. Briefly, bacteria were seeded onto 96-well disposable microtiter plates (SPL34096, SPL Life Sciences, Korea) and suspended particles were diluted to the indicated concentrations in 100 µL aliquots of TSB containing 10<sup>5</sup> CFU mL<sup>-1</sup> of bacteria. The MICs of particles (1.95–8000.00 µg mL<sup>-1</sup>) were determined after 24 h incubation at 37 °C. The cytotoxicities of the Ag-Te, Cu-Te, Te, Ag, and Cu particles were evaluated in HDF cells using MTT assays after 24 and 48 h incubation. In these experiments, cells were seeded at 10<sup>4</sup> cells per well in 96-well plates containing Dulbecco's modified Eagle's medium (Hyclone, GE Healthcare Biosciences, USA) supplemented with 10% fetal bovine serum, 50 IU mL<sup>-1</sup> penicillin, and 50 µg mL<sup>-1</sup> streptomycin, and were maintained at 37 °C in a humidified chamber containing 5% CO<sub>2</sub> for 12 h. After particle exposures, adherent cells were washed and incubated with 100 µL of MTT reagent (1.25 mg mL<sup>-1</sup>) for 4 h in the dark. The resulting formazan crystals were then dissolved in 100 µL of dimethyl sulfoxide, and the absorbance was recorded at 570 nm using a microplate reader (Multiskan EX, Thermo Scientific, USA). Cell viability was calculated as A<sub>sample</sub>/A<sub>control</sub> × 100%, where A is the absorbance at 570 nm. HDF cells were treated with particles at 50 µg mL<sup>-1</sup> for indicated times. Cellular ROS generation was then analyzed using 2',7'-dichlorodihydrofluorescein diacetate assays (ab113851, Abcam, UK) with a flow cytometer (BD Biosciences, USA). Blood samples were cannulated from male Sprague-Dawley rats and were centrifuged, and RBCs were then resuspended in saline (10×). RBC suspensions were then dispersed in normal saline or 0.025% Triton X-100 to obtain negative and positive controls, respectively. Subsequently, particle samples were added to RBC suspensions at 50 µL per mL, and were incubated at 37 ± 1 °C for 30 min followed by centrifugation at 4000 rpm for 10 min. Absorbance values of supernatants were then recorded at 540 nm using a microplate spectrophotometer (Multiskan EX,

Thermo Scientific, USA) and percentage hemolysis was calculated. Data are presented as means  $\pm$  standard deviation. Differences between treatment groups were identified using Student's *t*-test and one-way analysis of variance and were considered significant when  $p < 0.05$ . All animal procedures were performed in accordance with the Guidelines for Care and Use of Laboratory Animals of Yeungnam University and approved by the Institutional Animal Ethics Committee of Yeungnam University.

## Conflicts of interest

There are no conflicts to declare.

## Acknowledgements

This research was supported by Basic Science Research Program through the National Research Foundation of Korea (NRF) funded by the Ministry of Science, ICT and future Planning (NRF-2018R1A2A1A05020683).

## References

- 1 S. B. Levy and B. Marshall, Antibacterial resistance worldwide: Causes, challenges and responses, *Nat. Med.*, 2004, **10**, S122–S129.
- 2 L. B. Rice, The clinical consequences of antimicrobial resistance, *Curr. Opin. Microbiol.*, 2009, **12**, 476–481.
- 3 N. G. Durmus and T. J. Webster, Eradicating antibiotic-resistant biofilms with silver-conjugated superparamagnetic iron oxide nanoparticles, *Adv. Healthcare Mater.*, 2013, **2**, 165–171.
- 4 B. L. Ouay and F. Stellacci, Antibacterial activity of silver nanoparticles: A surface science insight, *Nano Today*, 2015, **10**, 339–354.
- 5 K. Zheng, M. I. Setyawati, D. T. Leong and J. Xie, Antimicrobial silver nanomaterials, *Coord. Chem. Rev.*, 2018, **357**, 1–17.
- 6 K. Zheng, M. I. Setyawati, D. T. Leong and J. Xie, Antimicrobial gold nanoclusters, *ACS Nano*, 2017, **11**, 6904–6910.
- 7 K. Zheng, M. I. Setyawati, T.-P. Lim, D. T. Leong and J. Xie, Antimicrobial cluster bombs: Silver nanoclusters packed with daptomycin, *ACS Nano*, 2016, **10**, 7934–7942.
- 8 Z.-M. Xiu, Q.-B. Zhang, H. L. Puppala, V. L. Colvin and P. J. J. Alvarez, Negligible particle-specific antibacterial activity of silver nanoparticles, *Nano Lett.*, 2012, **12**, 4271–4275.
- 9 C. Chen, P. Gunawan, X. W. Lou and R. Xu, Silver nanoparticles deposited layered double hydroxide nanoporous coatings with excellent antimicrobial activities, *Adv. Funct. Mater.*, 2012, **22**, 780–787.
- 10 S. Chernousova and M. Epple, Silver as antibacterial agent: Ion, nanoparticle, and metal, *Angew. Chem., Int. Ed.*, 2013, **52**, 1636–1653.
- 11 M. Rai, A. Yadav and A. Gade, Silver nanoparticles as a new generation of antimicrobials, *Biotechnol. Adv.*, 2009, **27**, 76–83.
- 12 H. L. Karlsson, P. Cronholm, J. Gustafsson and L. Möller, Copper oxide nanoparticles are highly toxic: A comparison between metal oxide nanoparticles and carbon nanotubes, *Chem. Res. Toxicol.*, 2008, **21**, 1726–1732.
- 13 L. K. Limbach, P. Wick, P. Manser, R. N. Grass, A. Bruinink and W. J. Stark, Exposure of engineered nanoparticles to human lung epithelial cells: Influence of chemical composition and catalytic activity on oxidative stress, *Environ. Sci. Technol.*, 2007, **41**, 4158–4163.
- 14 Y.-N. Chang, M. Zhang, L. Xia, J. Zhang and G. Xing, The toxic effects and mechanisms of CuO and ZnO nanoparticles, *Materials*, 2012, **5**, 2850–2871.
- 15 Y. Toduka, T. Toyooka and Y. Ibuki, Flow cytometric evaluation of nanoparticles using side-scattered light and reactive oxygen species-mediated fluorescence–Correlation with genotoxicity, *Environ. Sci. Technol.*, 2012, **46**, 7629–7636.
- 16 Z. Wang, L. Zhang, J. Zhao and B. Xing, Environmental processes and toxicity of metallic nanoparticles in aquatic systems as affected by natural organic matter, *Environ. Sci.: Nano*, 2016, **3**, 240–255.
- 17 K. Mijnendonckx, N. Leys, J. Mahillon, S. Silver and R. Van Houdt, Antimicrobial silver: Uses, toxicity and potential for resistance, *BioMetals*, 2013, **26**, 609–621.
- 18 P. T. Anastas and J. B. Zimmerman, Safer by design, *Green Chem.*, 2016, **18**, 4324.
- 19 E. Caballero-Díaz, C. Pfeiffer, L. Kastl, P. Rivera-Gil, B. Simonet, M. Valcárcel, J. Jiménez-Lamana, F. Laborda and W. J. Parak, The toxicity of silver nanoparticles depends on their uptake by cells and thus on their surface chemistry, *Part. Part. Syst. Charact.*, 2013, **30**, 1079–1085.
- 20 Y. Zhang, G. Hong, Y. Zhang, G. Chen, F. Li, H. Dai and Q. Wang, Ag<sub>2</sub>S quantum dot: A bright and biocompatible fluorescent nanoprobe in the second near-infrared window, *ACS Nano*, 2012, **6**, 3695–3702.
- 21 J. Liu, P. N. Duchesne, M. Yu, X. Jiang, X. Ning, R. D. Vinluan, P. Zheng and J. Zheng, Luminescent gold nanoparticles with size-independent emission, *Angew. Chem., Int. Ed.*, 2016, **55**, 8894–8898.
- 22 B. K. Paudel, K.-O. Doh and J. H. Byeon, Ag photoionization-induced single-pass assembly of Ag<sub>2</sub>S nanodots in flowing thiol droplets, *Green Chem.*, 2018, **20**, 978–983.
- 23 E. Burello and A. P. Worth, A rule for designing safer nanomaterials: Do not interfere with the cellular redox equilibrium, *Nanotoxicology*, 2015, **9**, 116–117.
- 24 S. Lin, T. Yu, Z. Yu, X. Hu and D. Yin, Nanomaterials safer-by-design: An environmental safety perspective, *Adv. Mater.*, 2018, **30**, 1705691.
- 25 S. George, S. Pokhrel, T. Xia, B. Gilbert, Z. Ji, M. Schowalter, A. Rosenauer, R. Damoiseaux, K. A. Bradley, L. Mädler and A. E. Nel, Use of a rapid cytotoxicity screening approach to engineer a safer zinc oxide nanoparticle through iron doping, *ACS Nano*, 2009, **4**, 15–29.
- 26 T. Xia, Y. Zhao, T. Sager, S. George, S. Pokhrel, N. Li, D. Schoenfeld, H. Meng, S. Lin, X. Wang, M. Wang, Z. Ji, J. I. Zink, L. Mädler, V. Castranova, S. Lin and A. E. Nel, Decreased dissolution of ZnO by iron doping yields

- nanoparticles with reduced toxicity in the rodent lung and zebrafish embryos, *ACS Nano*, 2011, 5, 1223–1235.
- 27 B. Sun, S. Pokhrel, D. R. Dunphy, H. Zhang, Z. Ji, X. Wang, M. Wang, Y.-P. Liao, C. H. Chang, J. Dong, R. Li, L. Mädler, C. J. Brinker, A. E. Nel and T. Xia, Reduction of acute inflammatory effects of fumed silica nanoparticles in the lung by adjusting silanol display through calcination and metal doping, *ACS Nano*, 2015, 9, 9357–9372.
  - 28 H. Naatz, S. Lin, R. Li, W. Jiang, Z. Ji, C. H. Chang, J. Köser, J. Thöming, T. Xia and A. E. Nel, Safe-by-design CuO nanoparticles via Fe-doping, Cu–O bond length variation, and biological assessment in cells and zebrafish embryos, *ACS Nano*, 2017, 11, 501–515.
  - 29 B. Zare, M. A. Faramarzi, Z. Sepehrizadeh, M. Shakibaie, S. Rezaie and A. R. Shahverdi, Biosynthesis and recovery of rod-shaped tellurium nanoparticles and their bactericidal activities, *Mater. Res. Bull.*, 2012, 47, 3719–3725.
  - 30 Z. H. Lin, C. H. Lee, H. Y. Chang and H. T. Chang, Antibacterial activities of tellurium nanomaterials, *Chem. – Asian J.*, 2012, 7, 930–934.
  - 31 H. Y. Chang, J. Cang, P. Roy, H. T. Chang, Y. C. Huang and C. C. Huang, Synthesis and antimicrobial activity of gold/silver–tellurium nanostructures, *ACS Appl. Mater. Interfaces*, 2014, 6, 8305–8312.
  - 32 E. Zonaro, S. Lampis, R. J. Turner, S. J. S. Qazi and G. Vallini, Biogenic selenium and tellurium nanoparticles synthesized by environmental microbial isolates efficaciously inhibit bacterial planktonic cultures and biofilms, *Front. Microbiol.*, 2015, 6, 584.
  - 33 A. K. Samal and T. Pradeep, Room-temperature chemical synthesis of silver telluride nanowires, *J. Phys. Chem. C*, 2009, 113, 13539–13544.
  - 34 A. Som and T. Pradeep, Heterojunction double dumbbell  $\text{Ag}_2\text{Te}$ – $\text{Te}$ – $\text{Ag}_2\text{Te}$  nanowires, *Nanoscale*, 2012, 4, 4537–4543.
  - 35 G. D. Moon, S. Ko, Y. Xia and U. Jeong, Chemical transformations in ultrathin chalcogenide nanowires, *ACS Nano*, 2010, 4, 2307–2319.
  - 36 H. Li, R. Brescia, M. Povia, M. Prato, G. Bertoni, L. Manna and I. Moreels, Synthesis of uniform disk-shaped copper telluride nanocrystals and cation exchange to cadmium telluride quantum disks with stable red emission, *J. Am. Chem. Soc.*, 2013, 135, 12270–12278.
  - 37 Y. Qiu, J. Ye, Y. Liu and X. Yang, Facile rapid synthesis of a nanocrystalline  $\text{Cu}_2\text{Te}$  multi-phase transition material and its thermoelectric performance, *RSC Adv.*, 2017, 7, 22558–22566.
  - 38 B. K. Poudel, J. H. Park and J. H. Byeon, On-demand gas-to-liquid process to fabricate thermoresponsive antimicrobial nanocomposites and coatings, *ACS Appl. Mater. Interfaces*, 2017, 9, 15342–15349.
  - 39 M. J. Hajipour, K. M. Fromm, A. A. Ashkarran, D. J. de Aberasturi, I. R. de Larramendi, T. Rojo, V. Serpooshan, W. J. Parak and M. Mahmoudi, Antibacterial properties of nanoparticles, *Trends Biotechnol.*, 2012, 30, 499–511.
  - 40 P. A. Lambert, Cellular impermeability and uptake of biocides and antibiotics in Gram-positive bacteria and mycobacteria, *J. Appl. Microbiol.*, 2002, 92, 46S–54S.
  - 41 J. S. Kim, E. Kuk, K. N. Yu, J. H. Kim, S. J. Park, H. J. Lee, S. H. Kim, Y. K. Park, Y. H. Park, C.-Y. Hwang, Y. K. Kim, Y. S. Lee, D. H. Jeong and M. H. Cho, Antimicrobial effects of silver nanoparticles, *Nanomedicine*, 2007, 3, 95–101.
  - 42 J. A. Lemire, J. J. Harrison and R. J. Turner, Antimicrobial activity of metals: Mechanisms, molecular targets and applications, *Nat. Rev. Microbiol.*, 2013, 11, 371–384.
  - 43 A. Panáček, L. Kvítek, M. Smékalová, R. Večeřová, M. Kolář, M. Röderová, F. Dyčka, M. Šebela, R. Prucek, O. Tomanec and R. Zbořil, Bacterial resistance to silver nanoparticles and how to overcome it, *Nat. Nanotechnol.*, 2018, 13, 65–71.
  - 44 M. M. H. C. M. Valko, H. Morris and M. T. D. Cronin, Metals, toxicity and oxidative Stress, *Curr. Med. Chem.*, 2005, 12, 1161–1208.
  - 45 P. Cronholm, H. L. Karlsson, J. Hedberg, T. A. Lowe, L. Winnberg, K. Elihn, I. O. Wallinder and L. Möller, Intracellular uptake and toxicity of Ag and CuO nanoparticles: A comparison between nanoparticles and their corresponding metal ions, *Small*, 2013, 9, 970–982.
  - 46 W. Li, R. Zamani, P. R. Gil, B. Pelaz, M. Ibáñez, D. Cadavid, A. Shavel, R. A. Alvarez-Puebla, W. J. Parak, J. Arbiol and A. Cabot, CuTe nanocrystals: Shape and size control, plasmonic properties, and use as SERS probes and photothermal agents, *J. Am. Chem. Soc.*, 2013, 135, 7098–7101.
  - 47 R. Foldbjerg, P. Olesen, M. Hougaard, D. A. Dang, H. J. Hoffmann and H. Autrup, PVP-coated silver nanoparticles and silver ions induce reactive oxygen species, apoptosis and necrosis in THP-1 monocytes, *Toxicol. Lett.*, 2009, 190, 156–162.
  - 48 J. H. Byeon, A. Kulkarni, H.-K. Kim, D. H. Thompson and J. T. Roberts, Photoassisted one-step aerosol fabrication of zwitterionic chitosan nanoparticles, *Biomacromolecules*, 2014, 15, 2320–2325.
  - 49 M. Slotte and R. Zevenhoven, Energy efficiency and scalability of metallic nanoparticle production using arc/spark discharge, *Energies*, 2017, 10, 1605–1623.